

Collective ionic dynamics in the liquid Na-Cs alloy: An *ab initio* molecular dynamics studyJ. Blanco,¹ D. J. González,^{1,2} L. E. González,¹ J. M. López,¹ and M. J. Stott²¹*Departamento de Física Teórica, Facultad de Ciencias, Universidad de Valladolid, 47011 Valladolid, Spain*²*Department of Physics, Queen's University, Kingston, Ontario, Canada K7L 3N6*

(Received 17 September 2002; published 21 April 2003)

We present results for several structural and dynamical properties of the liquid Na-Cs alloy. The study has been carried out by means of the orbital-free *ab initio* molecular dynamics method, combined with local ionic pseudopotentials constructed within the same framework. The results show good agreement with the available experimental data, reproducing the homocoordinating tendency exhibited by this alloy.

DOI: 10.1103/PhysRevE.67.041204

PACS number(s): 61.20.Ja, 61.25.Mv

I. INTRODUCTION

Molecular dynamics (MD) has become a useful technique to study the properties of liquid systems. The classical molecular dynamics (CMD) techniques require interatomic potentials, whereas the *ab initio* molecular dynamics (AIMD) methods compute the forces acting on the nuclei from electronic structure calculations performed as the MD trajectory is generated. Therefore the nuclear positions evolve according to classical mechanics, while the electronic subsystem follows adiabatically.

Recently, there have been many applications of the AIMD methods based on the density functional theory (DFT) [1,2]. This theory allows us to calculate the ground state electronic energy of a collection of atoms, for given nuclear positions, and yields the forces on the nuclei via the Hellmann-Feynman theorem. However, the computational demands of those AIMD methods where a Kohn-Sham (KS) orbital representation of DFT is used (KS-AIMD methods) grow very rapidly with the system size and limits the sizes of the systems and the simulation times [3–6]. These limitations can be partly overcome by the so-called orbital-free *ab initio* molecular dynamics (OF-AIMD) method which by eliminating the orbitals of the KS formulation provides a simulation method where the number of variables describing the electronic state is greatly reduced, enabling the study of larger samples (several hundreds of particles) and for longer simulation times (tens of picosecond).

The study of the dynamical properties of liquid metals has already produced much experimental and theoretical work [7]. Most experimental investigations have been performed by means of inelastic neutron scattering although the recent development of new synchrotron radiation has opened the possibility of using x rays too. It has also been stimulated by MD simulations because of its ability to determine several dynamical magnitudes that are not accessible to experiment, and, in this way, they have supplemented the experimental information. On the theoretical side, the development of microscopic theories such as the memory function formalism or the kinetic theory has created a theoretical framework, whose application to simple liquids has lead to good qualitative results for several dynamical magnitudes [7–9].

Less attention has been devoted to the dynamics of liquid binary alloys, although the last 15 years have witnessed an increasing effort. Following a CMD study of liquid Na-K

[10], the field was stimulated by a CMD simulation of liquid Li₄Pb by Jacucci *et al.* [11], where a new, high-frequency mode, supported by the Li atoms only (the so-called “fast sound”) was found. Subsequently, several theoretical [12–14], computer simulations [15–17] and experimental [16,18–20] studies have investigated the existence and properties of the collective excitations in liquid binary systems. For binary systems with disparate masses, two main branches (low- and high-frequency ones) of the collective excitations have been found to contribute to the longitudinal dynamics, although its origin is still unclear. However, the transverse dynamics has been much less investigated, mainly because it is not visible in scattering experiments and only the MD simulations can provide information about the transverse excitations. At this stage we mention that the recent application of the generalized collective model (GCM) approach, which combines CMD simulations with the memory function formalism, to binary Lennard-Jones fluids and liquid alloys has shown the existence of transverse optic modes that arise in connection with the concentration fluctuations.

This paper reports an AIMD study on the structural and dynamical properties of the liquid Na-Cs alloy. This system exhibits significant homocoordinating tendencies, and has already attracted much experimental [21–24] and theoretical [6,24–28] work. The experimental works have measured several thermodynamic magnitudes [21–23], as well as the static structure factor by means of x-ray-diffraction and neutron-diffraction experiments [24]. A marked departure from ideality has been observed in several properties; especially a substantial increase in the concentration fluctuation structure factor $S_{CC}(0)$, at sodium concentrations $x_{Na} \approx 0.8$. On the theoretical side, several studies using either semiempirical [25–28] or more fundamental [6,24] approaches have calculated the static structure and/or some thermodynamic magnitudes such as the concentration dependence of $S_{CC}(0)$ or the entropy of mixing which according to the experiment is nearly ideal. Among the semiempirical models, we mention Refs. [25–28] that calculated the concentration dependence of $S_{CC}(0)$ [25,26,28] and the free energy of mixing [25] or the entropy of mixing [26,27]. As for the more fundamental approaches, Huijben *et al.* [24] performed a CMD simulation using interatomic pair potentials obtained from the standard second-order pseudopotential perturbation theory. Their results predicted homocoordinating tendencies

although strongly overestimated the oscillations of the experimental total static structure factor. Recently, Costa Cabral and Martins [6] have performed an AIMD study, with ionic pseudopotentials derived by the Troullier-Martins method [29], to determine the static structure and the diffusion coefficients (DC's) in the alloy. Their results for the total static structure factor showed a good agreement with the experiment, although for $x_{\text{Na}}=0.8$ some discrepancies appeared for the amplitude of the oscillations. Moreover, because of the huge computational demands of their method, these authors used 108 particles and the simulation ranged for 400 configurations only, which obviously does not allow to study most of the dynamical magnitudes.

II. THEORY

A simple liquid metallic alloy $A_x B_{1-x}$ can be regarded as an assembly of N_A , A type, and N_B , B type, bare ions with charges Z_v^A and Z_v^B , respectively, interacting with $N_e = N_A Z_v^A + N_B Z_v^B$ valence electrons through electron-ion potentials $v_A(r)$ and $v_B(r)$. Therefore, the total potential energy of the system can be written, within the Born-Oppenheimer approximation, as the sum of the direct ion-ion interaction energy, which we assume Coulombic, and the ground state energy of the electronic system subject to the external potential created by the ions, $V_{\text{ext}}(\vec{r}, \{\vec{R}_l\}) = \sum_{i=A,B} \sum_{l(i)} v_i(|\vec{r} - \vec{R}_l|)$,

$$E(\{\vec{R}_l\}) = \frac{1}{2} \sum_{i,j=A,B} \sum_{l(i) \neq m(j)} \frac{Z_i Z_j}{|\vec{R}_l - \vec{R}_m|} + E_g[\rho_g(\vec{r}), V_{\text{ext}}(\vec{r}, \{\vec{R}_l\})], \quad (1)$$

where \vec{R}_l are the ionic positions, the sum over $l(i)$ extends over the sites occupied by the i -type ions, and $\rho_g(\vec{r})$ is the ground state electronic density. According to DFT, $\rho_g(\vec{r})$ can be obtained by minimizing the energy functional

$$E[\rho(\vec{r})] = T_s[\rho] + E_{\text{ext}}[\rho] + E_H[\rho] + E_{\text{xc}}[\rho], \quad (2)$$

where the terms represent, respectively, the electronic kinetic energy $T_s[\rho]$ of a noninteracting system with density $\rho(\vec{r})$, the energy of interaction with the external potential due to the ions,

$$E_{\text{ext}}[\rho] = \int d\vec{r} \rho(\vec{r}) V_{\text{ext}}(\vec{r}); \quad (3)$$

the classical electrostatic energy (Hartree term),

$$E_H[\rho] = \frac{1}{2} \int \int d\vec{r} d\vec{s} \frac{\rho(\vec{r}) \rho(\vec{s})}{|\vec{r} - \vec{s}|}; \quad (4)$$

and the exchange-correlation energy $E_{\text{xc}}[\rho]$ whose exact expression is unknown, although several approximations have been proposed. The simplest one is the so-called local density approximation (LDA),

$$E_{\text{xc}}^{\text{LDA}}[\rho] = \int d\vec{r} \rho(\vec{r}) \epsilon_{\text{xc}}(\rho(\vec{r})), \quad (5)$$

where $\epsilon_{\text{xc}}(\rho)$ is the density of exchange-correlation energy in a uniform electron gas of density ρ , which is known through simulations [30] and further fittings [31,32]. Although the LDA is clearly inexact, however, it is remarkable that hundreds of calculations with the LDA have yielded accurate calculated properties for many systems. This success is partially attributed to the fact that it gives the correct sum rule for the exchange-correlation hole [33]. Further improvements have been developed, which include dependence on the gradient of the density. However, because of its simplicity, most AIMD calculations have used the LDA, and we have also adopted it in the present calculations.

A. The kinetic energy functional

The kinetic energy functional T_s is a basic ingredient of the energy functional. It is generally considered [34] that the von Weizsäcker term

$$T_W[\rho(\vec{r})] = \frac{1}{8} \int d\vec{r} |\vec{\nabla} \rho(\vec{r})|^2 / \rho(\vec{r}) \quad (6)$$

is essential for a good description of the kinetic energy. It applies in the case of rapidly varying densities, and it is exact for one- or two-electron systems. Usually other terms are added in order to correctly reproduce some exactly known limits. In the uniform density limit, the exact kinetic energy is given by the Thomas-Fermi functional

$$T_{\text{TF}}[\rho(\vec{r})] = \frac{3}{10} \int d\vec{r} \rho(\vec{r}) k_F(\vec{r})^2, \quad (7)$$

where $k_F(\vec{r}) = (3\pi^2)^{1/3} \rho(\vec{r})^{1/3}$ is the local Fermi wave vector. In the limit of almost uniform density, the linear response theory (LRT) is correct, with a response function corresponding to a noninteracting uniform electron gas, which is given by the Lindhard function $\chi_L(q, \rho_0)$.

The computational advantages of the OF-AIMD method have stimulated the development of accurate kinetic energy functionals [35–38] which correctly recover some known limits, such as the Thomas-Fermi, the linear response, and the quadratic response limits. However, an undesirable feature of those functionals is that they are not positive definite, and therefore can lead to unphysical negative kinetic energies.

Within the ‘‘averaged density’’ approach, Chacón and co-workers [39,40] have developed some kinetic energy functionals that, besides recovering the uniform and LRT limits, are also positive definite. However, they are complicated to apply as they require order N more fast Fourier transforms (FFT's) than simpler functionals. Therefore we have used a simplified version [41],

$$T_s = T_W[\rho] + T_\beta[\rho], \quad (8)$$

$$T_\beta[\rho] = \frac{3}{10} \int d\vec{r} \rho(\vec{r})^{5/3-2\beta} \tilde{k}(\vec{r})^2, \quad (9)$$

$$\tilde{k}(\vec{r}) = (2k_F^0)^3 \int d\vec{s} k(\vec{s}) w_\beta(2k_F^0|\vec{r}-\vec{s}|),$$

$$k(\vec{r}) = (3\pi^2)^{1/3} \rho(\vec{r})^\beta,$$

where k_F^0 is the Fermi wave vector corresponding to a mean electron density ρ_0 and $w_\beta(x)$ is a weighting function, determined by requiring the correct recovery of the LRT and uniform density limits. This kinetic energy functional is positive definite for any value of β ; moreover, in the $k_F^0 \rightarrow 0$ limit when the mean electron density vanishes (e.g., for a finite system), the von Weizsäcker term is recovered if $\beta=4/9$, whereas for other values of β , the limit is $T_W + C^2 T_{TF}$. In the present simulations, we have used $\beta=0.51$, which is close to $4/9$ and for which $C=0.046$.

B. Pseudopotentials

We briefly describe the main steps in the construction of the ionic local pseudopotentials $v_{ps}(r)$ used to describe the ion-electron interaction; further details are in Refs. [41,42]. The pseudopotentials are developed from first principles by fitting to a generic model of an ion immersed in a metallic medium. In the first step [42], for a given ion type, the electron density distribution is calculated in a model system composed of an homogeneous electron gas of density $\rho_0 = N_e/V$, in which a spherical cavity has been made and where the ion has been inserted. This is performed using the KS-DFT approach and includes core and valence electron states. The latter are used to determine the change, $n^\alpha(r)$ ($\alpha=A,B$), in the valence electron density induced in the jellium by the presence of the α -type ion and the cavity (the displaced valence electron density). The $n^\alpha(r)$ is pseudized so as to eliminate the core-orthogonality oscillations. In the second step [41], an effective local pseudopotential $v_{ps}^\alpha(r)$ is constructed, so that when inserted into the jellium together with the cavity, it reproduces, *within* the OF-DFT procedure, the same pseudized $n^\alpha(r)$ as previously obtained. This is achieved by inserting each $n^\alpha(r)$ into the Euler equation, obtained by minimizing the energy functional of Eq. (2), together with the normalization constraint $\int_V d\vec{r} n^\alpha(r) = Z_v^\alpha$,

$$\frac{\delta T_s[\rho]}{\delta \rho(\vec{r})} + \frac{\delta E_{ext}[\rho]}{\delta \rho(\vec{r})} + \frac{\delta E_H[\rho]}{\delta \rho(\vec{r})} + \frac{\delta E_{xc}[\rho]}{\delta \rho(\vec{r})} - \mu = 0, \quad (10)$$

with $\rho(r) \equiv \rho^\alpha(r) = \rho_0 + n^\alpha(r)$ and $\mu \equiv \mu^\alpha$ is a Lagrange multiplier. Moreover, due to the spherical symmetry of the system, all the magnitudes depend on $|\vec{r}| \equiv r$.

C. Technical details

We have considered 600 ions in a cubic cell with periodic boundary conditions. Given the ionic positions at time t , the electronic energy functional is minimized with respect to $\rho(\vec{r})$, yielding the ground state electronic density and energy.

In order to keep $\rho(\vec{r}) \geq 0$ everywhere, the minimization is most conveniently performed in terms of an *effective orbital* $\psi(\vec{r})$, defined through $\rho(\vec{r}) = \psi(\vec{r})^2$, with real $\psi(\vec{r})$. This effective orbital is expanded in plane waves compatible with the simple cubic periodic boundary conditions of the simulation:

$$\begin{aligned} \psi(\vec{r}) &= \sum_{\vec{G}} c_{\vec{G}} e^{-i\vec{G}\cdot\vec{r}}, \\ c_{\vec{G}} &= \frac{1}{V} \int_V d\vec{r} \psi(\vec{r}) e^{i\vec{G}\cdot\vec{r}}, \\ \vec{G} &= \frac{2\pi}{L} (n_1, n_2, n_3), \end{aligned} \quad (11)$$

where L is the superlattice parameter, V is the volume of the cell, and the expansion is truncated at wave vectors corresponding to a given cutoff energy E_{Cut} . Following Car and Parrinello [43], we introduce a fictitious kinetic energy $\mathcal{T} = \frac{1}{2} M_c \sum_{\vec{G}} |dc_{\vec{G}}/dt|^2$, and determine the electronic ground state using damped Newtonian mechanics with an electronic time step Δt_c . We have used $M_c = 3.5 \times 10^7$ hartree a.u.³ and a $\Delta t_c = 1.1 \times 10^{-4}$ ps. The forces on the ions were obtained via the Hellmann-Feynman theorem, $\vec{F}_i = -\vec{\nabla}_{\vec{R}_i} E_g[\rho(\vec{r}), \{\vec{R}_i\}]$, ($i=1, \dots, N$) and the ionic positions and velocities were updated by numerically solving Newton's equations, $d^2\vec{R}_i/dt^2 = \vec{F}_i/M_i$, using the Verlet leapfrog algorithm [44] with a time step $\Delta t = 2.5 \times 10^{-3}$ ps. The $E_{\text{Cut}} = 10$ Ry and the calculation of properties was made averaging over 40 ps after an equilibration time of 4 ps.

III. RESULTS

A. Structural properties

The liquid Na-Cs alloy has been simulated for three thermodynamic states at $T=373$ K and concentrations $x_{\text{Na}} = 0.3, 0.5$, and 0.75 , with the experimental total ionic number densities taken from Refs. [25,26].

The simulations allow a direct evaluation of the partial pair distribution functions $g_{ij}(r)$, which are shown in Fig. 1, and the partial Ashcroft-Langreth (AL) structure factors $S_{ij}(q)$. The $g_{\text{Na-Na}}(r)$ changes substantially with concentration, whereas both $g_{\text{Na-Cs}}(r)$ and $g_{\text{Cs-Cs}}(r)$ change little. As the Na concentration is increased, the height of the main peak of $g_{\text{Na-Na}}(r)$ decreases, whereas those for $g_{\text{Na-Cs}}(r)$ and $g_{\text{Cs-Cs}}(r)$ are relatively unchanged and slightly smaller, respectively. Also, for $x_{\text{Na}} = 0.30$ and 0.50 , the $g_{\text{Na-Cs}}(r)$ remains smaller than the average of $g_{\text{Cs-Cs}}(r)$ and $g_{\text{Na-Na}}(r)$, which is an indication of homocoordinating tendencies.

The Warren-Cowley [45–47] short range order (SRO) parameter for the first neighbor shell, $\alpha_1^{(i)}$, is a simple way of displaying the short range order in the alloy. It is defined as

$$\alpha_1^{(i)} = 1 - \frac{n_{ij}}{x_j(n_{ii} + n_{ij})} \quad (j \neq i = 1, 2), \quad (12)$$

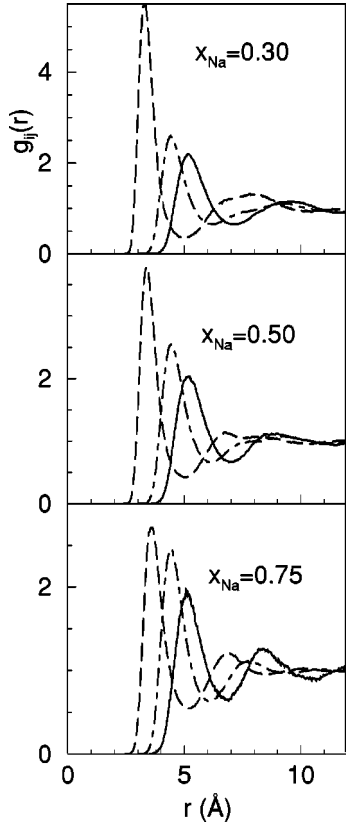


FIG. 1. Partial pair distribution functions $g_{ij}(r)$ for the liquid Na-Cs alloy at $T=373$ K and three concentrations. The full, dashed, and dot-dashed lines represent the $g_{\text{Cs-Cs}}(r)$, $g_{\text{Na-Na}}(r)$, and $g_{\text{Na-Cs}}(r)$, respectively.

where n_{ij} is the number of j -type particles around an i -type particle, within a sphere of radius R_{ij} . The n_{ij} can be calculated from the $g_{ij}(r)$ by

$$n_{ij} = 4\pi\rho x_j \int_0^{R_{ij}} r^2 g_{ij}(r) dr, \quad (13)$$

where R_{ij} is usually identified [48] as the position of the first minimum of $g_{ij}(r)$. For a random distribution of atoms, $\alpha_1^{(i)} = 0$, whereas a positive (negative) value for $\alpha_1^{(i)}$ suggests homocoordinating (heterocoordinating) tendency. Calculated values for $\alpha_1^{(\text{Na})}$ and $\alpha_1^{(\text{Cs})}$ for the liquid $\text{Na}_x\text{Cs}_{1-x}$ alloy at $T=373$ K are shown in Table I, but they are inconclusive since $\alpha_1^{(\text{Cs})}$ is always positive whereas $\alpha_1^{(\text{Na})}$ is negative.

TABLE I. Calculated values of coordination numbers n_{ij} and the Warren-Cowley SRO parameters $\alpha_1^{(i)}$ for the Na-Cs liquid alloy at $T=373$ K. The numbers in parenthesis give the values of $\alpha_1^{(i)}$ when n_{ij} are evaluated by integrating up to the position of the first minimum of $g_{\text{Cs-Cs}}(r)$.

x_{Na}	$n_{\text{Na-Na}}$	$n_{\text{Na-Cs}}$	$n_{\text{Cs-Na}}$	$n_{\text{Cs-Cs}}$	$\alpha_1^{(\text{Na})}$	$\alpha_1^{(\text{Cs})}$
0.30	2.4	7.3	3.4	10.8	-0.08 (0.04)	0.21 (0.015)
0.50	4.0	6.4	6.4	8.5	-0.23 (0.01)	0.14 (0.0)
0.75	7.6	4.0	11.9	5.1	-0.38 (0.04)	0.07 (0.0)

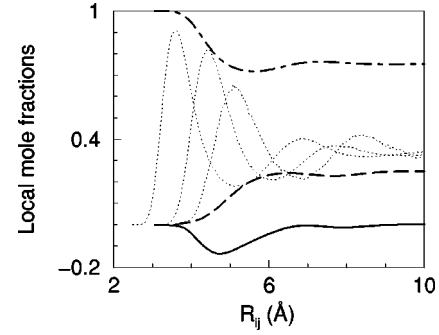


FIG. 2. Local mole fractions $x_{\text{Na-Na}}$ (dot-dashed line), $x_{\text{Cs-Cs}}$ (dashed line), and $x_s - 1$ (full line), as function of the upper integration limit R_{ij} , for the liquid $\text{Na}_{0.75}\text{Cs}_{0.25}$ alloy at $T=373$ K. The dotted lines represent the partials $g_{\text{Na-Na}}(r)$, $g_{\text{Na-Cs}}(r)$, and $g_{\text{Cs-Cs}}(r)$, scaled so as to fit in the figure.

However, the Warren-Cowley SRO parameters may be inadequate because of the large atomic size mismatch between the pure components (the volume ratio is around 3.0), and we have resorted to the local mole fractions method [49–53] that has also been widely used to study the homocoordinating tendencies in mixtures. For a binary system, the local mole fractions x_{ii} are defined as

$$x_{ii} = \frac{n_{ii}}{n_{ii} + n_{ij}}, \quad j \neq i = 1, 2. \quad (14)$$

Since there has been much discussion [49,54–56] of the suitable upper integration limit R_{ij} in Eq. (13), we have evaluated x_{ii} as a function of R_{ij} . For an homogeneous phase, when both species are nearly equally distributed, $x_s - 1 = x_{11} + x_{22} - 1$ is around zero; whereas for a demixed state particles of the same species dominate the distribution and $x_s - 1$ grows [50,51]. Figure 2 shows, for $x_{\text{Na}}=0.75$, a plot of $x_s - 1$ as a function of the upper integration limit R_{ij} in Eq. (13). Notice that x_s , x_{11} , and x_{22} change rapidly when R_{ij} increases, but a plateau is observed when R_{ij} reaches values around the position of the first minimum of the $g_{\text{Cs-Cs}}(r)$. Taking this minimum as the upper integration limit R_{ij} , $x_s - 1$ takes small positive values, suggesting a weak homocoordinating tendency. Furthermore, the corresponding Warren-Cowley SRO parameters now become positive (see Table I). The total static structure factor at several concentrations and temperatures has been measured using x-ray-diffraction and neutron-diffraction experiments by van der Lugt and co-workers [24]. Several experimental x-ray and neutron weighted total static structure factors $S_T(q)$ are shown in Fig. 3 along with the OF-AIMD simulation results that reproduce rather well the basic features of the measured $S_T(q)$, namely, the position and amplitude of the oscillations, including the damping of the oscillations with increasing sodium concentration. From the experimental x ray and neutron $S_T(q)$'s, and assuming $S_{\text{Na-Na}}(q) \approx 1$, van der Lugt and co-workers [24] derived semiempirical results for $S_{\text{Cs-Cs}}(q)$ and $S_{\text{Na-Cs}}(q)$. Their results for $x_{\text{Na}}=0.30$ are shown in Fig. 4 along with the OF-AIMD simulations that partly support the $S_{\text{Na-Na}}(q) \approx 1$ assumption, although notice-

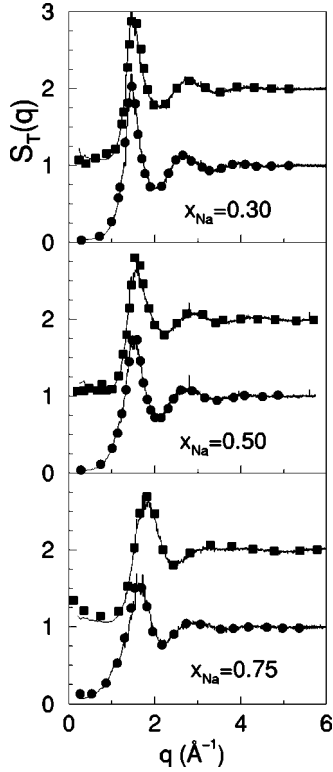


FIG. 3. Total static structure factor $S_T(q)$ for the liquid Na-Cs alloy at $T=373$ K and three concentrations. Continuous lines are the results from the present OF-AIMD simulations, whereas the full circles and squares are the experimental x-ray-diffraction and neutron diffraction-data, respectively. The neutron data have been shifted upward by one unit.

able deviations appear at $q \approx 1.35 \text{ \AA}^{-1}$, where its first minimum is located. Discrepancies in $S_{\text{Na-Cs}}(q)$ also appear in this region, but for other q 's the agreement between the semiempirical/simulation results for $S_{\text{Cs-Cs}}(q)$ and $S_{\text{Na-Cs}}(q)$ is satisfactory. The recent AIMD simulations [6] for $x_{\text{Na}}=0.60$ and 0.80 also gave reasonable results for $S_{ij}(q)$ and $S_T(q)$, although a detailed comparison with the experiment is not possible because the results are rather noisy (due to the small sample size and simulation time).

For investigating the ordering tendencies in a liquid alloy, the Bhatia-Thornton (BT) partial structure factors [57] are ideally suited. For a binary alloy, they are the concentration-concentration [$S_{\text{CC}}(q)$], the number-number [$S_{\text{NN}}(q)$], and the number-concentration [$S_{\text{NC}}(q)$] partial structure factors, defined as

$$S_{\text{CC}}(q) = x_1 x_2 [x_2 S_{11}(q) + x_1 S_{22}(q) - 2(x_1 x_2)^{1/2} S_{12}(q)],$$

$$S_{\text{NN}}(q) = x_1 S_{11}(q) + x_2 S_{22}(q) + 2(x_1 x_2)^{1/2} S_{12}(q),$$

$$S_{\text{NC}}(q) = S_{11}(q) - S_{22}(q) + (x_2 - x_1)/(x_1 x_2)^{1/2} S_{12}(q),$$

where $S_{ij}(q)$ are the AL partial structure factors. Moreover, their long-wavelength limit provides microscopic information on the liquid alloy, e.g., $S_{\text{CC}}(q \rightarrow 0)$ portrays short range order. The experimental results [22–24] for $S_{\text{CC}}(q \rightarrow 0)/x_{\text{Na}}x_{\text{Cs}}$ are slightly greater than unity for $0 \leq x_{\text{Na}} \leq 0.5$,

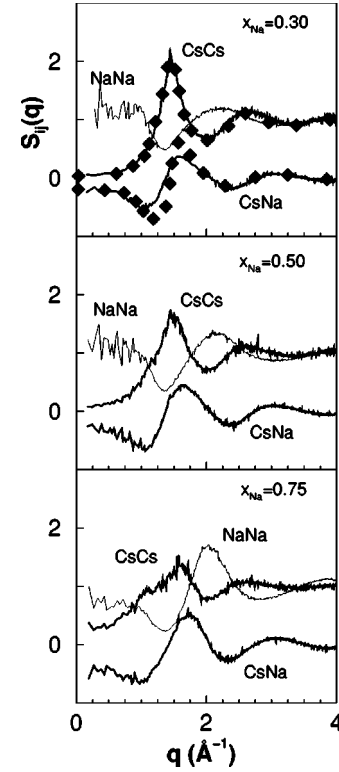


FIG. 4. Partial static structure factors $S_{ij}(q)$ for the liquid Na-Cs alloy at $T=373$ K and three concentrations. The full diamonds are semiexperimental data of Huijben *et al.* [24].

≤ 0.5 , then increase toward a maximum value of ≈ 7 at $x_{\text{Na}}=0.80$ and thereafter quickly decrease toward 1. These values clearly indicate homocoordinating tendencies for all concentrations. Although this behavior is qualitatively reproduced by the present OF-AIMD simulations, the results for $S_{\text{CC}}(q \rightarrow 0)/x_{\text{Na}}x_{\text{Cs}}$ remain around ≈ 1.3 with a minimum value of ≈ 1.0 for $x_{\text{Na}} \approx 0.50$.

B. Dynamic properties

1. Single-particle dynamics

The information about the transport properties in multi-component liquid systems is provided by various time correlation functions among the atomic velocities. However, they cannot be determined experimentally and must be obtained by other methods such as MD simulation. We present results for the relative velocity correlation functions (VCF) $Z_{ij}(t)$ defined [58] as the time correlation function of the relative velocity of the center of mass of species i with respect to that of species j :

$$Z_{ij}(t) = \frac{1}{3} x_i x_j N \langle [\vec{u}_i(t) - \vec{u}_j(t)] \cdot [\vec{u}_i(0) - \vec{u}_j(0)] \rangle, \quad (15)$$

where N is the total number of particles and $\vec{u}_i(t)$ the mean velocity of component i , is given in terms of the velocity of the i -type particle $l(i)$, $\vec{u}_{l(i)}(t)$, as

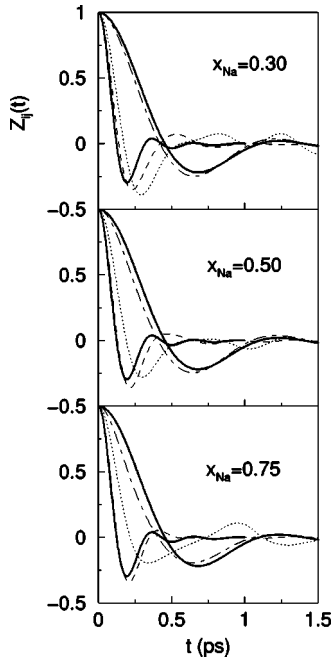


FIG. 5. Normalized self- and relative VCF's for the liquid Na-Cs alloy at $T=373$ K and three concentrations. The dashed, dot-dashed, and dotted lines represent the $Z_{\text{Na}}^s(t)$, $Z_{\text{Cs}}^s(t)$, and $Z_{\text{Na-Cs}}(t)$, respectively. The full thick lines represent the VCF's of pure Na (fast decay) and Cs (slower decay) at $T=373$ K.

$$\vec{u}_i(t) \equiv (x_i N)^{-1} \sum_{l(i)=1}^{N_i} \vec{u}_{l(i)}(t). \quad (16)$$

The $Z_{ij}(t)$ can be separated into self- $[Z_{ij}^0(t)]$, and distinct, $[Z_{ij}^d(t)]$, contributions which reflect the self-dynamic and cross-dynamic correlations, and give information about the mobility of particles and the coupling between the velocities of distinct particles, respectively,

$$Z_{ij}(t) = (1 - \delta_{ij}) Z_{ij}^0(t) + x_i x_j Z_{ij}^d(t), \quad (17)$$

where δ_{ij} is Kronecker's delta. In terms of the well-known velocity autocorrelation function $Z_i^s(t) = \frac{1}{3} \langle \vec{u}_{1i}(t) \vec{u}_{1i}(0) \rangle$ of a tagged i -type particle in the fluid, we write $Z_{ij}^0(t) = x_j Z_i^s(t) + x_i Z_j^s(t)$. The $Z_{ij}^d(t)$ account for the contribution of the distinct velocity correlations. The time integrals of $Z_{ij}(t)$, $Z_{ij}^0(t)$, $Z_{ij}^d(t)$, and $Z_i^s(t)$ give the associated DC's, namely D_{ij} , D_{ij}^0 , D_{ij}^d , and D_i^s , respectively, where D_i^s is the usual self-diffusion coefficient. Simplifications for the binary mixtures give

$$D_{12} = D_{12}^0 + x_1 x_2, \quad D_{12}^d \equiv D_{12}^0 (1 + \gamma_{12}), \quad (18)$$

with $D_{12}^0 = x_2 D_1^s + x_1 D_2^s$ and γ_{12} is the measure of the deviation from an ideal mixture, vanishing when species are the same. Finally, we note that the interdiffusion coefficient is written as

$$D_{\text{int}} = \theta D_{12} \equiv \theta (1 + \gamma_{12}) D_{12}^0, \quad (19)$$

TABLE II. Input data for the series Na-Cs at $T=373$ K, studied in this work, along with some simulation details. ρ is the total ionic number density taken from Ref. [25,26].

$x = x_{\text{Na}}$	ρ (\AA^{-3})	Cutoff(Ry)
0.0	0.008111	10.0
0.30	0.010564	10.0
0.50	0.012897	10.0
0.75	0.017132	10.0
1.0	0.024221	10.0

where $\theta = x_1 x_2 / S_{\text{CC}}(q \rightarrow 0)$. For a nearly ideal mixture, $\theta \approx 1$, $\gamma_{12} \approx 0$ and consequently $D_{\text{int}} \approx D_{12}^0$.

The results for the self- and relative VCF for $\text{Na}_x \text{Cs}_{1-x}$ liquid alloy are shown in Fig. 5, along with the corresponding quantities for both pure Na and Cs at $T=373$ K and number densities at their corresponding coexisting lines (see Table II). First, we note that $Z_{\text{Na}}^s(t)$ and $Z_{\text{Cs}}^s(t)$ have shapes (rate of decay and depth of first minimum) similar to the pure components. However, due to the large mass difference between the Na and Cs ions, the Na ions in the alloy will experience, during the collisions, larger relative changes in their velocities than the Cs ions. This is reflected in their VCF, with $Z_{\text{Cs}}^s(t)$ exhibiting a slower decay and smaller backscattering than the $Z_{\text{Na}}^s(t)$. Moreover, as x_{Na} increases, the backscattering effect is slightly reduced because of fewer collisions with the Cs ions, tending to enhance the corresponding self-diffusion coefficient D_{Na}^s , an effect that is somewhat counterbalanced by the increase in the total number density.

The $Z_{\text{Na-Cs}}(t)$ lies between $Z_{\text{Na}}^s(t)$ and $Z_{\text{Cs}}^s(t)$ suggesting that distinct correlation effects are weak; in fact the contribution of distinct effects to $D_{\text{Na-Cs}}$ is usually measured by $\gamma_{\text{Na-Cs}}$ Eq. (18). For all concentrations, we obtain small positive values of $\gamma_{\text{Na-Cs}}$, which as shown in Table III are smaller than 10%. Moreover, the positive values of $D_{\text{Na-Cs}}^d$ indicate [58,59] that particles of the same species have a greater tendency to diffuse together than those of distinct species, another indicator of homocoordinating tendencies in the alloy. These tendencies are weaker at $x_{\text{Na}} \approx 0.5$, where the values of both $\gamma_{\text{Na-Cs}}$ and $D_{\text{Na-Cs}}^d$ reach minima.

The experimental determination of the self-diffusion coefficients in metallic melts is rather difficult and, to our

TABLE III. Diffusion coefficients (in 10^{-4} cm^2/s), and related quantities for the Na-Cs liquid alloy at $T=373$ K.

x_{Na}	0.30	0.50	0.75
D_{Na}^s	0.41	0.39	0.48
D_{Cs}^s	0.34	0.31	0.32
$D_{\text{Na-Cs}}$	0.42	0.36	0.38
$D_{\text{Na-Cs}}^0$	0.39	0.34	0.36
$D_{\text{Na-Cs}}^d$	0.16	0.08	0.09
$\gamma_{\text{Na-Cs}}$	0.09	0.06	0.07
D_{int}	0.327	0.363	0.371

knowledge, have only been measured for the Na-K system for 32% sodium at several temperatures [60]. As a check on the accuracy of our results, we have also calculated the self-diffusion coefficients of the pure components at 373 K. Results are $D_{\text{Na}}^0 = 0.48$ and $D_{\text{Cs}}^0 = 0.39$, which compare favorably with the corresponding experimental values [61] of 0.42 and 0.39 (10^{-4} cm²/s units), respectively. The AIMD simulation of Costa Cabral and Martins [6] gave somewhat smaller values for D_{Cs}^s and D_{Na}^s , which may be a consequence of the small number of particles and short time used in their simulations.

2. Collective dynamics

The collective dynamics of density fluctuations in the alloy is usually described through the partial intermediate scattering functions $F_{ij}(\vec{q}, t) = \langle \rho_i(\vec{q}, t) \cdot \rho_j^*(\vec{q}, 0) \rangle$, where the asterisk denotes the complex conjugation and

$$\rho_j(\vec{q}, t) = \frac{1}{\sqrt{N_j}} \sum_{l(j)=1}^{N_j} \exp[i\vec{q} \cdot \vec{R}_{l(j)}(t)] \quad (20)$$

is the density fluctuation of the j th component with wave vector \vec{q} , in which $\vec{R}_{l(j)}(t)$ is the position of the j -type particle $l(j)$ and $\langle \dots \rangle$ denotes the ensemble average. The time Fourier transform of the $F_{ij}(\vec{q}, t)$ into the frequency domain leads to the partial dynamic structure factors $S_{ij}(\vec{q}, \omega)$, which are directly related to the inelastic neutron scattering data. Associated with the density fluctuations is the j th component particle current

$$\vec{j}_j(\vec{q}, t) = \frac{1}{\sqrt{N_j}} \sum_{l=1}^{N_j} \vec{u}_{l(j)}(t) \exp[i\vec{q} \cdot \vec{R}_{l(j)}(t)], \quad (21)$$

which is usually split into a longitudinal component $j_j^L(\vec{q}, t)$, parallel to \vec{q} , and a transverse component $j_j^T(\vec{q}, t)$, perpendicular to \vec{q} . The partial longitudinal, $C_{ij}^L(\vec{q}, t)$, and transverse, $C_{ij}^T(\vec{q}, t)$, current correlation functions are obtained from these through

$$C_{ij}^L(\vec{q}, t) = \langle j_i^L(\vec{q}, t) j_j^{L*}(\vec{q}, 0) \rangle, \quad (22)$$

$$C_{ij}^T(\vec{q}, t) = \frac{1}{2} \langle j_i^T(\vec{q}, t) j_j^{T*}(\vec{q}, 0) \rangle.$$

The corresponding time Fourier transforms give the associated spectra, $C_{ij}^L(\vec{q}, \omega) = \omega^2 S_{ij}(\vec{q}, \omega)$ and $C_{ij}^T(\vec{q}, \omega)$, respectively. Finally, we note that for isotropic systems all these correlation functions depend only on $q = |\vec{q}|$.

Figures 6 and 7 show, for two q values, the partial intermediate scattering functions $F_{\text{Cs-Cs}}(q, t)$, $F_{\text{Na-Na}}(q, t)$, and $F_{\text{Na-Cs}}(q, t)$, as well as the BT partial intermediate scattering functions $F_{\text{NN}}(q, t)$ and $F_{\text{CC}}(q, t)$. $F_{\text{Cs-Cs}}(q, t)$, $F_{\text{Na-Na}}(q, t)$, $F_{\text{NN}}(q, t)$, and $F_{\text{CC}}(q, t)$ are always positive, whereas $F_{\text{Na-Cs}}(q, t)$ can have either sign. This is consistent with $S_{\text{Na-Cs}}(q)$ oscillating about zero, since $F_{ij}(q, t=0) = S_{ij}(q)$. The $F_{ij}(q, t)$ go monotonically to zero, showing slower de-

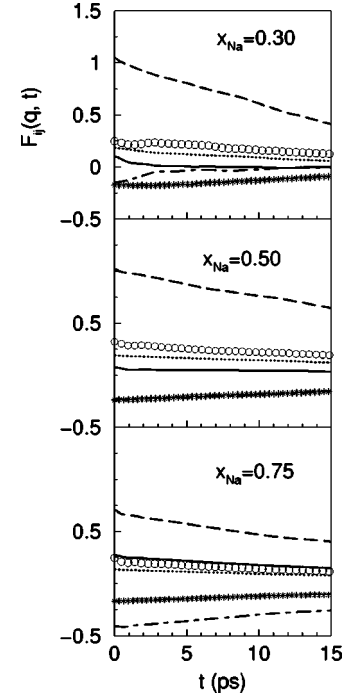


FIG. 6. Partial intermediate scattering functions $F_{ij}(q, t)$ at $q = 0.27 \text{ \AA}^{-1}$, or the liquid Na-Cs alloy at $T = 373 \text{ K}$ and three concentrations. The full, dashed, dot-dashed lines, circles, stars, and dotted lines represent $F_{\text{Cs-Cs}}(q, t)$, $F_{\text{Na-Na}}(q, t)$, $F_{\text{Na-Cs}}(q, t)$, $F_{\text{NN}}(q, t)$, $F_{\text{NC}}(q, t)$, and $F_{\text{CC}}(q, t)$, respectively.

cays for the smaller q 's. In the hydrodynamic regime ($q \rightarrow 0$), the decay of $F_{ij}(q, t)$ for binary mixtures is related to both entropy and concentration fluctuations, and the slow decay observed in Fig. 6 is mainly due to diffusion effects resulting from concentration fluctuations.

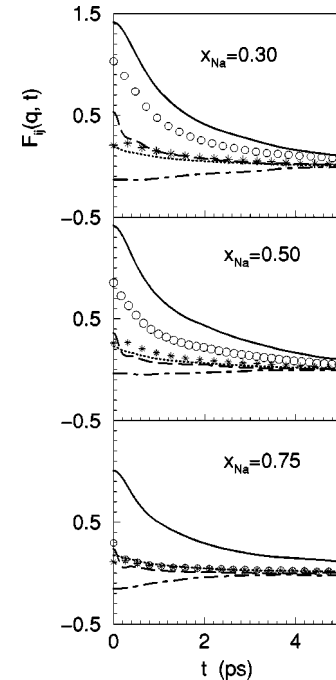


FIG. 7. Same as Fig. 6, but for $q = 1.34 \text{ \AA}^{-1}$.

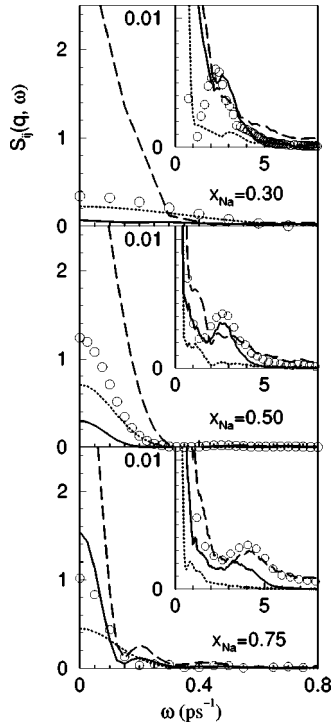


FIG. 8. Partial dynamic structure factors $S_{ij}(q, \omega)$, at $q = 0.27 \text{ \AA}^{-1}$, for the liquid Na-Cs alloy at $T = 373 \text{ K}$ and three concentrations. The full, dashed, circles, and dotted lines represent the $S_{\text{Cs-Cs}}(q, \omega)$, $S_{\text{Na-Na}}(q, \omega)$, $S_{\text{NN}}(q, \omega)$, and $S_{\text{CC}}(q, \omega)$, respectively.

The $S_{ij}(q, \omega)$ also provide information concerning the microscopic mechanisms of propagating longitudinal modes, e.g., the peaks in $S_{\text{Li-Li}}(q, \omega)$ for the Li_4Pb liquid alloy have been related to propagating fast modes supported by the Li ions. Figures 8 and 9 show results for $S_{\text{Cs-Cs}}(q, \omega)$, $S_{\text{Na-Na}}(q, \omega)$, $S_{\text{NN}}(q, \omega)$, and $S_{\text{CC}}(q, \omega)$. For the smaller q 's and all concentrations, $S_{\text{Cs-Cs}}(q, \omega)$, $S_{\text{Na-Na}}(q, \omega)$, and $S_{\text{NN}}(q, \omega)$ exhibit clear side peaks that for $q \leq 0.20 \text{ \AA}^{-1}$ are located at very similar frequencies; this is the typical behavior of $S_{ij}(q, \omega)$ in the hydrodynamic regime and represents a propagating sound mode.

The range of existence of the side peaks or shoulders depends on the concentration, with the majority component exhibiting a wider range. For the $\text{Na}_{0.3}\text{Cs}_{0.7}$ alloy, both $S_{\text{Cs-Cs}}(q, \omega)$ and $S_{\text{NN}}(q, \omega)$ show side peaks up to $q \approx 0.90 \text{ \AA}^{-1}$, at which point they shoulder and vanish for $q \geq 1.0 \text{ \AA}^{-1}$. Meanwhile, $S_{\text{Na-Na}}(q, \omega)$ has side peaks up to $q \approx 0.40 \text{ \AA}^{-1}$, and shoulders up to $q \approx 0.85 \text{ \AA}^{-1}$. For the $\text{Na}_{0.75}\text{Cs}_{0.25}$ alloy, both $S_{\text{Na-Na}}(q, \omega)$ and $S_{\text{NN}}(q, \omega)$ have side peaks or shoulders up to $q \approx 1.40 \text{ \AA}^{-1}$, while in $S_{\text{Cs-Cs}}(q, \omega)$ they appear only up to $q \approx 0.50 \text{ \AA}^{-1}$.

The $S_{\text{NN}}(q, \omega)$ reflects the average behavior of the system and in the limit of a binary mixture of identical species, $S_{\text{NN}}(q, \omega)$ reduces to the usual dynamic structure factor of a one-component system. Therefore, it is not surprising that in the hydrodynamic regime, $S_{\text{NN}}(q, \omega)$ exhibits a clear Rayleigh-Brillouin structure [62], similar to that of the dynamic structure factor in one-component liquids. Our results show Brillouin peaks (see insets of Fig. 8) for small q values, which become remnant shoulders for larger q and eventually

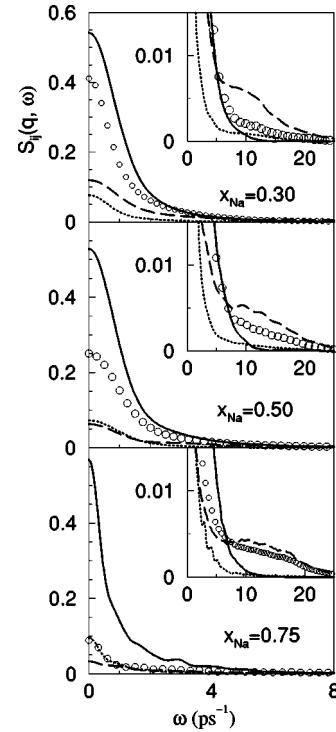


FIG. 9. Same as Fig. 8, but for $q = 1.34 \text{ \AA}^{-1}$.

disappear. These Brillouin peaks at small q 's are associated with acoustic modes propagating through the binary alloy with adiabatic velocity of propagation, $c_s = \omega_B/q$, where ω_B is the position of the Brillouin peak. For the concentration $x_{\text{Na}} = 0.30$, $S_{\text{NN}}(q = 0.23, \omega)$ shows a clear Brillouin peak at $\omega_B \approx 2.45 \text{ ps}^{-1}$ giving $c_s = 1065 \text{ m/s}$, which compares well with the observed value [63] of 1070 m/s. Similarly, we obtain $c_s = 1100 \text{ m/s}$ for $x_{\text{Na}} = 0.50$ and $c_s = 1480 \text{ m/s}$ for $x_{\text{Na}} = 0.75$, which are close to the experimental values [63] of ≈ 1160 and 1450 m/s , respectively. For the limits $x_{\text{Na}} = 1$ (pure Na) and $x_{\text{Na}} = 0$ (pure Cs), we obtain $c_s = 2450 \text{ m/s}$ and $c_s = 940 \text{ m/s}$, respectively, which also compare well with the corresponding experimental values [63] of 2520 and 960 m/s.

No clear side peaks have been observed in $S_{\text{CC}}(q, \omega)$, but shoulders appear which become weaker as q increases, and vanish for $q \geq 1.0 \text{ \AA}^{-1}$. This absence of concentration modes in $S_{\text{CC}}(q, \omega)$ can be attributed to the dominance of diffusive contributions in the partial intermediate scattering functions. However, such modes may be apparent in the associated partial longitudinal current correlation function $C_{\text{CC}}^L(q, \omega)$ because of the ω^2 factor that kills the low-frequency components and enhances the higher ones. Further information about the longitudinal collective modes can be obtained from the longitudinal current correlation functions $C_{ij}^L(q, \omega)$. These we have also evaluated, and Figs. 10 and 11 show results for $C_{\text{Cs-Cs}}^L(q, \omega)$, $C_{\text{Na-Na}}^L(q, \omega)$, $C_{\text{Na-Cs}}^L(q, \omega)$, $C_{\text{NN}}^L(q, \omega)$, and $C_{\text{CC}}^L(q, \omega)$.

For all q 's, $C_{\text{Cs-Cs}}^L(q, \omega)$, $C_{\text{Na-Na}}^L(q, \omega)$, and $C_{\text{NN}}^L(q, \omega)$ have at least one peak whose frequency coincides, at very small q 's, with that of the Brillouin peak in their respective $S_{\text{Cs-Cs}}(q, \omega)$, $S_{\text{Na-Na}}(q, \omega)$, and $S_{\text{NN}}(q, \omega)$. From those fre-

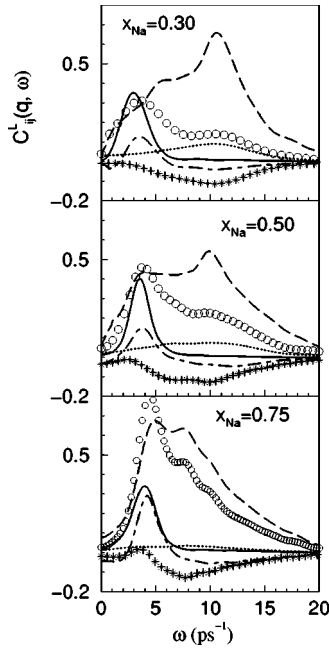


FIG. 10. Partial longitudinal current correlation functions $C_{ij}^L(q, \omega)$, at $q=0.27 \text{ \AA}^{-1}$, for the liquid Na-Cs alloy at $T=373 \text{ K}$ and three concentrations. The full, dashed, dot-dashed, circles, stars, and dotted lines represent $C_{\text{Cs-Cs}}^L(q, \omega)$, $C_{\text{Na-Na}}^L(q, \omega)$, $C_{\text{Na-Cs}}^L(q, \omega)$, $C_{\text{NN}}^L(q, \omega)$, $C_{\text{NC}}^L(q, \omega)$, and $C_{\text{CC}}^L(q, \omega)$, respectively.

quencies, the longitudinal dispersion relations $\omega_{\text{Cs-Cs}}^L(q)$, $\omega_{\text{Na-Na}}^L(q)$, and $\omega_{\text{NN}}^L(q)$ are obtained (see Fig. 12). Note that $\omega_{\text{Cs-Cs}}^L(q)$ always takes markedly smaller values than those of $\omega_{\text{Na-Na}}^L(q)$, due to the large atomic mass difference. For the three concentrations, $\omega_{\text{Cs-Cs}}^L(q)$ has one branch and $\omega_{\text{Na-Na}}^L(q)$ has two, with the lower one present only at small q 's, including the hydrodynamic region, and at frequencies

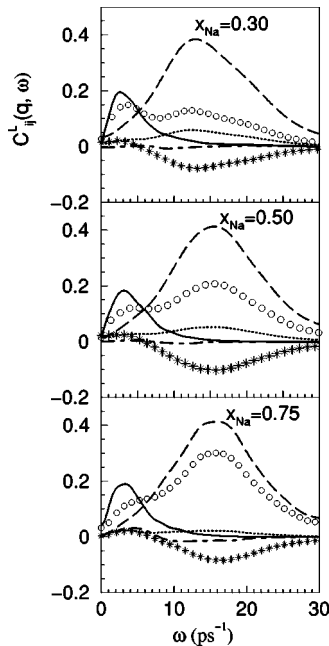


FIG. 11. Same as Fig. 10, but for $q=1.34 \text{ \AA}^{-1}$.

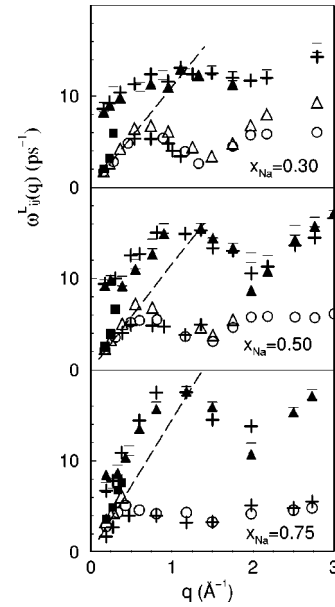


FIG. 12. Longitudinal dispersion relation of the partials, $\omega_{\text{Na-Na}}^L(q)$ (open and full squares), $\omega_{\text{Cs-Cs}}^L(q)$ (open circles), number-number $\omega_{\text{NN}}^L(q)$ (open and full triangles), and concentration-concentration $\omega_{\text{CC}}^L(q)$ (pluses) longitudinal modes for the Na-Cs liquid alloy at $T=373 \text{ K}$ and several concentrations. The slope of the dashed straight lines stands for the respective experimental sound velocity [63].

close to that of $\omega_{\text{Cs-Cs}}^L(q)$; and the higher one is present at frequencies comparable to those of the pure Na system. In the binary alloy, the heavy Cs ions have a characteristic low frequency, and the light Na ions a much higher frequency that persists up to the hydrodynamic regime, although for smaller q some Na ions start to oscillate with the Cs ions. In the hydrodynamic limit, all the particles must oscillate at the same frequency, and only the lower-frequency peak will survive in $C_{\text{Na-Na}}^L(q, \omega)$. The marked differences between $\omega_{\text{Cs-Cs}}^L(q)$, and $\omega_{\text{Na-Na}}^L(q)$, for most q 's, suggest that the motions of the Na and Cs ions are largely uncorrelated.

As shown in Fig. 12, at small q 's, the $\omega_{\text{Cs-Cs}}^L(q)$ has an initial linear increase up to a maximum followed by a minimum at $q \approx 1.5 \text{ \AA}^{-1}$, which corresponds to the main peak position of $S_{\text{Cs-Cs}}(q)$. As x_{Na} increases, the main peak of $S_{\text{Cs-Cs}}(q)$ drops, widens, and maintains its position at $\approx 1.5 \text{ \AA}^{-1}$; this explains that at the same time the first minimum of $\omega_{\text{Cs-Cs}}^L(q)$ becomes less marked while the first maximum moves toward smaller q values. A similar behavior is exhibited by the high-frequency branch of $\omega_{\text{Na-Na}}^L(q)$, with a maximum and minimum at same positions as those of $S_{\text{Na-Na}}(q)$. Moreover, as x_{Na} is increased the structure of $\omega_{\text{Na-Na}}^L(q)$ becomes more marked as it happens with the maxima and minima in $S_{\text{Na-Na}}(q)$.

The $\omega_{\text{NN}}^L(q)$ dispersion curve also has two branches because for some q region, the $C_{\text{NN}}^L(q, \omega)$ exhibits two peaks. As the $C_{\text{Na-Cs}}^L(q, \omega)$ is substantially smaller than the other partial currents, the behavior of the $C_{\text{NN}}^L(q, \omega)$ is dominated by $C_{\text{Cs-Cs}}^L(q, \omega)$ and $C_{\text{Na-Na}}^L(q, \omega)$, with the latter one playing a greater role even when Na is the minority component.

Therefore, as q decreases, $C_{NN}^L(q, \omega)$ shows two peaks, induced by the high-frequency peak of $C_{Na-Na}^L(q, \omega)$ and that of $C_{Cs-Cs}^L(q, \omega)$, respectively. At the hydrodynamic regime, the high-frequency peak disappears and only the low-frequency one remains that comes from the corresponding Brillouin peak in the $S_{NN}(q, \omega)$. Therefore, the two branches of $\omega_{NN}^L(q)$ are closely connected with $\omega_{Cs-Cs}^L(q)$ and with the high-frequency $\omega_{Na-Na}^L(q)$ branches, respectively. Moreover, the high-frequency $\omega_{NN}^L(q)$ branch disappears in the hydrodynamic regime, whereas the low-frequency branch exhibits now a linear behavior similar to that of $\omega_{Cs-Cs}^L(q)$.

Two branches are also exhibited by the $\omega_{CC}^L(q)$ dispersion curve because $C_{CC}^L(q, \omega)$, which is substantially small as compared with the other partial currents, shows either one or two peaks that may be connected with propagating concentration modes. At small q 's, including the hydrodynamic regime, $C_{CC}^L(q, \omega)$ shows only one peak, but for greater wave vectors two maxima appear in $C_{CC}^L(q, \omega)$: one at a similar frequency as the high-frequency branch of $C_{NN}^L(q, \omega)$ and another at a frequency slightly lower than that in $C_{Cs-Cs}^L(q, \omega)$. In conclusion, the high-frequency branch of $\omega_{CC}^L(q)$ exists for all q values, closely follows the high frequency $\omega_{NN}^L(q)$ and goes toward a finite value when $q \rightarrow 0$; this is a typical trend of the kinetic modes. On the other hand, the low-frequency branch of $\omega_{CC}^L(q)$ appears outside the hydrodynamic regime and closely follows $\omega_{Cs-Cs}^L(q)$.

3. Transverse currents

The partial transverse current correlation functions $C_{ij}^T(q, \omega)$ provide information about the existence of shear modes in the system. These modes are not associated directly with any measurable quantity and can only be analyzed by either theoretical models or by MD simulations. Few works have addressed the transverse currents in liquids, and most of them have focused on one-component systems where $C^T(q, \omega)$ evolves [7], as a function of ω , from a Gaussian (when $q \rightarrow \infty$) toward a Lorentzian curve (when $q \rightarrow 0$). Transverse modes do not propagate in these extreme regimes but at intermediate q 's, the $C^T(q, \omega)$ may exhibit a peak associated with propagating shear waves.

The first CMD simulations of transverse current correlations in binary fluids were performed on molten salts [64]. $C_{NN}^T(q, \omega)$ showed a peak at intermediate q 's as in one-component liquids. Also, a peak appeared in the charge-charge transverse current correlation functions at both small and intermediate q 's, which was related to transverse optic modes with a finite value of frequency in the hydrodynamic limit. Subsequent CMD studies in binary Lennard-Jones systems [14] and metallic alloys [65] have found opticlike modes associated with $C_{CC}^T(q, \omega)$.

Figures 13 and 14 show some calculated $C_{ij}^T(q, \omega)$. Both $C_{Cs-Cs}^T(q, \omega)$ and $C_{Na-Cs}^T(q, \omega)$ show no peaks for the smallest q 's reached in the simulations ($q_{min} \approx 0.19, 0.17,$ and 0.16 \AA^{-1} for $x_{Na}=0.75, 0.50,$ and 0.30 , respectively), however, starting from a q_c ($q_c \approx 0.23 \text{ \AA}^{-1}$ for $\text{Na}_{0.75}\text{Cs}_{0.25}$ and $q_c \approx 0.32 \text{ \AA}^{-1}$ for $\text{Na}_{0.3}\text{Cs}_{0.7}$) a peak appears in both partials, which persists for a limited range of q values. In contrast,

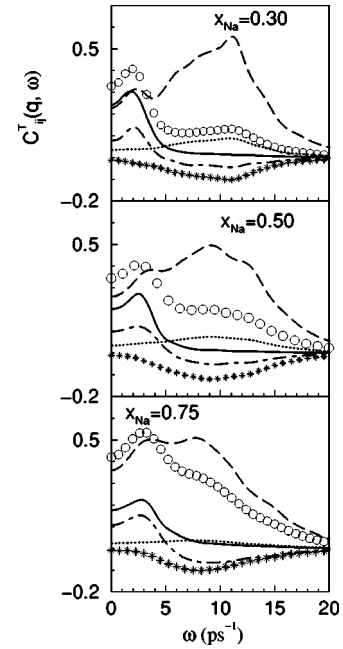


FIG. 13. Partial transverse current correlation functions $C_{ij}^T(q, \omega)$, at $q=0.43 \text{ \AA}^{-1}$, for the liquid Na-Cs alloy at $T=373 \text{ K}$ and three concentrations. The full, dashed, dot-dashed lines, circles, stars, and dotted lines represent $C_{Cs-Cs}^T(q, \omega)$, $C_{Na-Na}^T(q, \omega)$, $C_{Na-Cs}^T(q, \omega)$, $C_{NN}^T(q, \omega)$, $C_{NC}^T(q, \omega)$, and $C_{CC}^T(q, \omega)$, respectively.

$C_{Na-Na}^T(q, \omega)$ already exhibits a high-frequency peak at q_{min} , which lasts up to $q \approx 4 \text{ \AA}^{-1}$; moreover, a low-frequency peak appears in $C_{Na-Na}^T(q, \omega)$ at q_c , which persists for a limited range and has a similar frequency to those in $C_{Cs-Cs}^T(q, \omega)$ and $C_{Na-Cs}^T(q, \omega)$. Notice that $C_{Na-Cs}^T(q, \omega)$ quickly diminishes as q increases (see Figs. 13 and 14), in-

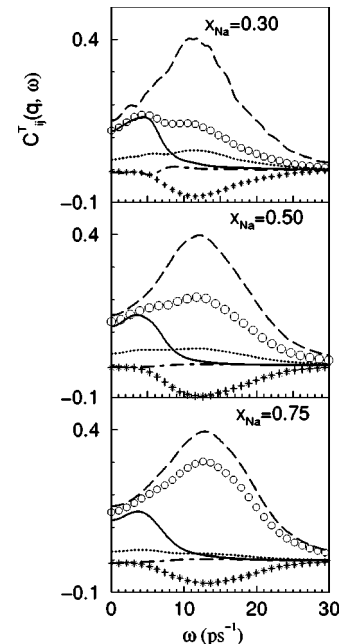


FIG. 14. Same as Fig. 13, but for $q=1.34 \text{ \AA}^{-1}$.

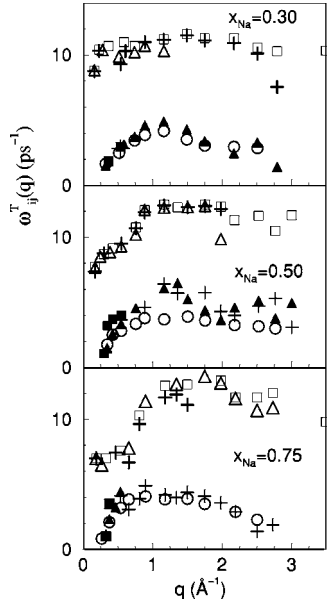


FIG. 15. Transverse dispersion relation of the partials, $\omega_{\text{Na-Na}}^T(q)$ (open and full squares), $\omega_{\text{Cs-Cs}}^T(q)$ (open circles), number-number $\omega_{\text{NN}}^T(q)$ (open and full triangles), and concentration-concentration $\omega_{\text{CC}}^T(q)$ (pluses) transverse modes for the Na-Cs liquid alloy at $T = 373$ K and several concentrations.

dicating strong decoupling of the dynamics of the two species.

From the peaks in $C_{ij}^T(q, \omega)$, the transverse dispersion relations $\omega_{ij}^T(q)$ are obtained (Fig. 15). $\omega_{\text{Cs-Cs}}^T(q)$ has one branch only, whereas $\omega_{\text{Na-Na}}^T(q)$ has two, with the lower-frequency branch staying rather close to $\omega_{\text{Cs-Cs}}^T(q)$. The appearance of the two branches in the dispersion relation of the lighter species was found earlier in the longitudinal dispersion relation, and is typical of binary systems with a significant mass ratio.

The $C_{\text{NN}}^T(q, t)$ gives information on the average behavior of the system. At q_{min} , it already shows a high-frequency peak similar to that of $C_{\text{Na-Na}}^T(q, \omega)$, moreover, a second peak appears for a limited range and shows a behavior typical of a one-component system. Consequently, the dispersion curve, $\omega_{\text{NN}}^T(q)$, has two branches: a high-frequency branch taking a finite value as $q \rightarrow 0$, and a low-frequency branch with a linear behavior for very small q values and going to zero as $q \rightarrow q_c$. In this linear region the low-frequency branch is quite close to $\omega_{\text{Cs-Cs}}^T(q)$ and to the low-frequency $\omega_{\text{Na-Na}}^T(q)$ branch, which suggests that the propagation of shear modes involves both species, although the appearance of the high-frequency branch of $\omega_{\text{Na-Na}}^T(q)$ shows that some Na particles exhibit kinetic modes in this low q region. Similar behavior was found in the longitudinal dispersion curves in the region within and close to the hydrodynamic regime. The appearance of the two branches for the $\omega_{\text{NN}}^T(q)$ is qualitatively different from the recent CMD simulations of Anento and Padró [65] for liquid Li-Mg, Li-Na and Li_4Pb alloys, where the $\omega_{\text{NN}}^T(q)$ had one branch only. Their $\omega_{\text{NN}}^T(q)$ in Li-Na, and Li-Mg alloys exhibited behavior qualitatively similar to the present low-frequency $\omega_{\text{NN}}^T(q)$ branch, whereas $\omega_{\text{NN}}^T(q)$

for the Li_4Pb alloy behaved similarly to the present high-frequency branch, remaining finite as $q \rightarrow 0$. This absence of the propagating transverse collective modes for the Li_4Pb alloy was associated [65] with the large mass ratio (≈ 30) of the components along with a majority concentration of the light Li particles. In the Na-Cs system, the mass ratio ≈ 6 , and we find two $\omega_{\text{NN}}^T(q)$ branches for the three concentrations considered. As the concentration of the light Na particles is increased, the high frequency $\omega_{\text{NN}}^T(q)$ branch exists for a larger q -range, while the range of the low-frequency $\omega_{\text{NN}}^T(q)$ branch shrinks toward smaller q values.

A fitting of the low-frequency $\omega_{\text{NN}}^T(q)$ branch in the linear region, $\omega_{\text{NN}}^T(q) \sim c_T(q - q_c)$, allows estimation of the velocity of propagation of the shear modes in the alloy: $c_T \approx 570$, ≈ 850 , and ≈ 1500 m/s for $x_{\text{Na}} = 0.30$, 0.50 , and 0.75 , respectively. For comparison, we have also calculated the velocities of the shear modes in pure Na and Cs at the same temperature, 373 K, obtaining $c_T \approx 1700$ m/s (pure Na) and $c_T \approx 475$ m/s (pure Cs).

$C_{\text{CC}}^T(q, \omega)$ is smaller than any of the other $C_{ij}^T(q, \omega)$, suggesting a weak contribution of concentration fluctuations to the collective transverse dynamics; however, clear peaks are seen in $C_{\text{CC}}^T(q, \omega)$. At q_{min} , there is a high-frequency peak for a limited q region, it takes finite values as $q \rightarrow 0$ and follows roughly the high-frequency $\omega_{\text{Na-Na}}^T(q)$ branch. This behavior has also been observed in molten salts, and was associated not with shear propagating modes but with transverse optic modes of kinetic character [14,64]. The damping of the concentration modes estimated from peak widths does not go to zero as $q \rightarrow 0$. Bryk, Mryglod, and Kahl [14], in their GCM study of transverse dynamics in the liquid Kr-Ar, $\text{Mg}_{0.7}\text{Zn}_{0.3}$, Li_4Pb , and $\text{He}_{0.75}\text{Ar}_{0.25}$ systems, reported similar results that they attributed to opticlke nature of the transverse concentration fluctuations. This conclusion was corroborated by Anento and Padró [65] in their CMD simulations of liquid Li-based alloys.

$\omega_{\text{CC}}^T(q)$ also has a low-frequency branch in a limited q range, starting at $q \approx 0.6 \text{ \AA}^{-1}$, outside the hydrodynamic region and even beyond the linear region associated with the shear modes. Its disappearance for $q \leq 0.6 \text{ \AA}^{-1}$ is further evidence of the homocoordinating tendencies of the liquid Na-Cs alloy [14,65].

In the hydrodynamic limit [7], the one-component transverse current correlation function $C^T(q, t)$ becomes

$$C^T(q \rightarrow 0, t) = (1/\beta m) \exp\{-q^2 \eta |t|/m\rho\}, \quad (23)$$

where β is the inverse temperature times the Boltzmann's constant, m is the mass of the particles, and η is the shear viscosity coefficient. For finite q , using the memory function representation,

$$\tilde{C}^T(q, z) = \frac{1}{\beta m} \left[z + \frac{q^2}{\rho m} \tilde{\eta}(q, z) \right]^{-1}, \quad (24)$$

where the tilde denotes the Laplace transform and $\tilde{\eta}(q, z)$ is a generalized shear viscosity coefficient. The area under the normalized $C^T(q, t)$ gives $\beta m \tilde{C}^T(q, z=0)$, from which val-

TABLE IV. Calculated and experimental values of the shear viscosity η (in GPa ps) for the Na-Cs liquid alloy at $T=373$ K.

x_{Na}	η	$\eta_{\text{expt.}}$
0.0	4.2 ± 0.5	4.7 ± 0.3^a
0.30	4.6 ± 0.5	
0.50	4.7 ± 0.5	
0.75	5.0 ± 0.5	
1.0	5.4 ± 0.5	6.6 ± 0.3^a

^aReference [66].

ues for $\tilde{\eta}(q, z=0)$ can be obtained and, when extrapolated to $q=0$, give the shear viscosity η . The results for η obtained in this way for pure Na and Cs at $T=373$ K are presented in Table IV, showing good agreement with the experiment [66]. Extension of this scheme to binary systems is straightforward. The equivalent correlation function is the total transverse current correlation function $C_{tt}^T(q, t) = \langle j_i^T(q, t) j_i^{T*}(q, 0) \rangle$, where $j_i^T(q, t) = x_1^{1/2} m_1 j_1^T(q, t) + x_2^{1/2} m_2 j_2^T(q, t)$ is the total transverse current and $j_i^T(q, t)$ are defined according to Eq. (21). In the hydrodynamic limit,

$$C_{tt}^T(q \rightarrow 0, t) = (\bar{m}/\beta) \exp\{-q^2 \eta |t| / \bar{m} \rho\}, \quad (25)$$

where $\bar{m} = x_1 m_1 + x_2 m_2$ and η is the alloy shear viscosity. The results for the alloy shear viscosity calculated in this way are presented in Table IV. No experimental results are available.

The viscosity of simple liquid alloys shows either a linear or slightly concave behavior with concentration, whereas large positive deviations from linearity are exhibited by liquid alloys with heterocoordinating tendencies [47,67]. When homocoordinating tendencies are present, the available experimental data suggest a mixed behavior, with a marked predominance for a negative departure from linearity. Moreover, some semiempirical models [47,67] establish a close connection between positive (negative) deviations from the linear law and a negative (positive) enthalpy of mixing in the alloy. The positive experimental enthalpy of mixing of Na-Cs alloy [21] suggests some negative deviation of the alloy shear viscosity from the linear law. The calculated values obtained for the shear viscosity of the liquid Na-Cs alloy, given in Table IV, show a linear variation with concentration, which according to the previous comments may reflect the real behavior of the system in view of its weak homocoordinating tendencies.

IV. CONCLUSIONS

Several static and dynamic properties of the liquid Na-Cs alloy have been calculated for three concentrations. The simulations have been performed using the orbital-free *ab initio* molecular dynamics method combined with first prin-

ciples local pseudopotentials derived within the same framework. This demonstrates the feasibility of this technique for investigating time correlation functions and the dynamical properties of binary alloys.

The results for the static structural properties show good agreement with the available experimental data, although the simulations predict somewhat weaker homocoordinating tendencies. We have analyzed the local arrangement of particles in the mixture and found that when there is a large size mismatch, the biggest value of the minimum of the $g_{ij}(r)$'s should be used for estimating the coordination numbers.

For the dynamical properties, we have analyzed several time correlation functions, although comparison with the experiment could only be made at the level of some transport coefficients. The excellent agreement with the experiment of the calculated self-diffusion coefficients for the pure components suggests that the simulations of the alloys treats self-diffusion very well. The calculated longitudinal dispersion relations show the existence of kinetic concentration modes. In addition, the results for the adiabatic sound velocity in the pure components and the alloy are in very good agreement with the experiment.

An interesting feature is the appearance of the two branches in the transverse dispersion relation for $\omega_{\text{NN}}^T(q)$, $\omega_{\text{Na-Na}}^T(q)$, and $\omega_{\text{CC}}^T(q)$, with the high-frequency branch representing overdamped kinetic modes. The low-frequency $\omega_{\text{NN}}^T(q)$ and $\omega_{\text{Na-Na}}^T(q)$ branches, along with the $\omega_{\text{Cs-Cs}}^T(q)$, go linearly to zero at a finite q value q_c and represent propagating shear modes. However, the low-frequency $\omega_{\text{CC}}^T(q)$ branch does not exist for low q values, in agreement with the predictions of the GCM model. The presence of two branches contrasts with the recent results for other binary systems [65], where only one branch for $\omega_{\text{NN}}^T(q)$ was found.

The shear viscosity of the alloy has been estimated by using its relationship with the hydrodynamic limit of the total transverse current correlation function. The results seem plausible, given the weak homocoordinating tendencies and the positive enthalpy of mixing of the alloy.

The main approximations in the orbital-free *ab initio* molecular dynamics method used here are the kinetic energy functional and the local pseudopotentials describing the electron-ion interactions. Further improvements in the method will come from the development of more accurate kinetic energy functionals, which would lead to improved local pseudopotentials.

ACKNOWLEDGMENTS

This work has been supported by the Junta de Castilla y León (Project No. VA 073/02) and the DGES (Project No. PB98-0641-C02-01). D.J.G. acknowledges the financial support of the Spanish Ministry of Education, Culture and Sports, and the University of Valladolid. M.J.S. acknowledges the support of the NSERC of Canada.

- [1] P. Hohenberg and W. Kohn, Phys. Rev. **136**, 864 (1964).
- [2] W. Kohn and L.J. Sham, Phys. Rev. **140**, A1133 (1965).
- [3] F. Shimojo, Y. Zempo, K. Hoshino, and M. Watabe, J. Non-Cryst. Solids **205**, 983 (1996); B.J. Costa Cabral and J.L. Martins, Phys. Rev. B **51**, 872 (1995).
- [4] G. Kresse, J. Non-Cryst. Solids **205**, 833 (1996); G. Kresse and J. Hafner, Phys. Rev. B **55**, 7539 (1997).
- [5] Y. Senda, F. Shimojo, and K. Hoshino, J. Phys. Soc. Jpn. **67**, 2753 (1998).
- [6] B.J. Costa Cabral and J.L. Martins, J. Chem. Phys. **111**, 5067 (1999).
- [7] U. Balucani and M. Zoppi, *Dynamics of the Liquid State* (Clarendon, Oxford, 1994); J.P. Hansen and I.R. McDonald, *Theory of Simple Liquids* (Academic, London, 1986); J.P. Boon and S. Yip, *Molecular Hydrodynamics* (McGraw-Hill, New York 1980).
- [8] L. Sjögren and A. Sjölander, J. Phys. C **12**, 4369 (1979); L. Sjögren, *ibid.* **13**, 705 (1980); Phys. Rev. A **22**, 2866 (1980); **22**, 2883 (1980).
- [9] J. Casas, D.J. González, L.E. González, M.M.G. Alemany, and L.J. Gallego, Phys. Rev. B **62**, 12 095 (2000).
- [10] G. Jacucci and I.R. McDonald, J. Phys. F: Met. Phys. **10**, L15 (1980).
- [11] G. Jacucci, M. Ronchetti, and W. Schirmacher, J. Phys. Colloq. **8**, 385 (1984).
- [12] A. Campa and E.G.D. Cohen, Phys. Rev. A **41**, 5451 (1990).
- [13] P. Westerhuijs, W. Montfrooij, L.A. de Graaf, and I.M. de Schepper, Phys. Rev. A **45**, 3749 (1992).
- [14] T. Bryk, I. Mryglod, and G. Kahl, Phys. Rev. E **56**, 2903 (1997); T. Bryk and I. Mryglod, Phys. Lett. A **261**, 349 (1999); J. Phys.: Condens. Matter **12**, 6063 (2000).
- [15] E. Enciso, N.G. Almarza, P. Dominguez, M.A. González, and F.J. Bermejo, Phys. Rev. Lett. **74**, 4233 (1995).
- [16] R.M. Crevecoeur, H.E. Smorenburg, and I.M. de Schepper, J. Low Temp. Phys. **105**, 149 (1996).
- [17] R. Fernandez-Perea, M. Alvarez, F.J. Bermejo, P. Verkerk, B. Roessli, and E. Enciso, Phys. Rev. E **58**, 4568 (1998).
- [18] W. Montfrooij, P. Westerhuijs, V.O. de Haan, and I.M. de Schepper, Phys. Rev. Lett. **63**, 544 (1989).
- [19] P.H.K. de Jong, P. Verkerk, C.F. de Vroege, L.A. de Graaf, W.S. Howells, and S.M. Bennington, J. Phys.: Condens. Matter **6**, L681 (1994).
- [20] M. Alvarez, F.J. Bermejo, P. Verkerk, and B. Roessli, Phys. Rev. Lett. **80**, 2141 (1998).
- [21] F. Yokokawa and O.J. Kleppa, J. Chem. Phys. **40**, 46 (1964).
- [22] K. Ichikawa, S.M. Grandstaff, and J.C. Thomson, J. Chem. Phys. **61**, 4059 (1974).
- [23] F.E. Neale and N.E. Cusack, J. Phys. F: Met. Phys. **12**, 2839 (1982).
- [24] M.J. Huijben, W. van der Lugt, W.A.M. Reimert, J.Th.M. de Hosson, and C. van Dijk, Physica B & C **97**, 338 (1979).
- [25] E.G. Visser, W. van der Lugt, and J.Th.M. de Hosson, J. Phys. F: Met. Phys. **10**, 1681 (1980).
- [26] F.E. Neale and N.E. Cusack, Phys. Chem. Liq. **14**, 115 (1984).
- [27] J.A. Alonso and L.J. Gallego, J. Phys. F: Met. Phys. **15**, L185 (1985).
- [28] K. Hoshino, J. Phys.: Condens. Matter **2**, 7345 (1990).
- [29] N. Troullier and J.L. Martins, Phys. Rev. B **43**, 1993 (1991).
- [30] D.M. Ceperley and B.J. Alder, Phys. Rev. Lett. **45**, 566 (1980).
- [31] S.H. Vosko, L. Wilk, and M. Nussair, Can. J. Phys. **58**, 1200 (1980).
- [32] J.P. Perdew and A. Zunger, Phys. Rev. B **23**, 5048 (1981).
- [33] D.C. Langreth and J.P. Perdew, Phys. Rev. B **15**, 2884 (1977).
- [34] E.S. Kryachko and E.V. Ludeña, *Energy Density Functional Theory of Many-Electron Systems* (Kluwer Academic, London, 1990), and references therein.
- [35] F. Perrot, J. Phys.: Condens. Matter **6**, 431 (1994).
- [36] E. Smargiassi and P.A. Madden, Phys. Rev. B **49**, 5220 (1994).
- [37] M. Foley and P.A. Madden, Phys. Rev. B **53**, 10 589 (1996).
- [38] Y.A. Wang, N. Govind, and E.A. Carter, Phys. Rev. B **58**, 13 465 (1998); **60**, 16 350 (1999).
- [39] E. Chacón, J.E. Alvarells, and P. Tarazona, Phys. Rev. B **32**, 7868 (1985).
- [40] P. Garcia-González, J.E. Alvarells, and E. Chacón, Phys. Rev. A **54**, 1897 (1996); Phys. Rev. B **53**, 9509 (1996); **57**, 4857 (1998).
- [41] L.E. González, D.J. González, and J.M. López, J. Phys.: Condens. Matter **13**, 7801 (2001).
- [42] L.E. González, A. Meyer, M.P. Iñiguez, D.J. González, and M. Silbert, Phys. Rev. E **47**, 4120 (1993).
- [43] R. Car and M. Parrinello, Phys. Rev. Lett. **55**, 2471 (1985).
- [44] See, for instance, M.P. Allen and D.J. Tildesley, *Computer Simulation of Liquids* (Oxford University Press, Oxford, 1987).
- [45] B.E. Warren, *X-Ray Diffraction* (Addison-Wesley, Reading MA, 1969).
- [46] J.M. Cowley, Phys. Rev. **77**, 667 (1950).
- [47] R.N. Singh and F. Sommer, Rep. Prog. Phys. **60**, 57 (1997).
- [48] R.L. McGreevy, A. Baranyai, and I. Ruff, Phys. Chem. Liq. **16**, 47 (1986).
- [49] K. Nakanishi, S. Okazaki, K. Ikari, T. Iguchi, and H. Tanaka, J. Chem. Phys. **76**, 629 (1982).
- [50] M. Schoen and C. Hoheisel, Mol. Phys. **53**, 1367 (1984).
- [51] P. Borgelt, C. Hoheisel, and G. Stell, J. Chem. Phys. **92**, 6161 (1990).
- [52] C. Rey, L.J. Gallego, L.E. González, and D.J. González, J. Chem. Phys. **97**, 5121 (1992).
- [53] M.C. Abramo, C. Caccamo, and G. Giunta, Phys. Rev. A **34**, 3279 (1986).
- [54] C. Hoheisel and F. Kohler, Fluid Phase Equilib. **16**, 13 (1984).
- [55] L.L. Lee, T.H. Chung, and K.E. Starling, Fluid Phase Equilib. **12**, 105 (1983).
- [56] R.G. Rubio, M.G. Prolongo, M. Diaz-Peña, and J.A.R. Renuncio, J. Phys. Chem. **91**, 1177 (1987).
- [57] A.B. Bhatia and D.E. Thornton, Phys. Rev. B **2**, 3004 (1970).
- [58] J. Trullás and J.A. Padró, J. Chem. Phys. **99**, 3983 (1993); Phys. Rev. E **50**, 1162 (1994).
- [59] T. Kato, J. Phys. Chem. **89**, 5750 (1985).
- [60] A. Feinauer and G. Majer, Phys. Rev. B **64**, 134302 (2001).
- [61] M. Gerl and A. Bruson, in *Handbook of Thermodynamic and Transport Properties of Alkali Metals*, edited by R.W. Oshe (Blackwell, Oxford, 1985), p. 843.
- [62] N.H. March and M.P. Tosi, *Atomic Dynamics in Liquids* (Dover Publications, New York, 1991).
- [63] M.G. Kim and S.V. Letcher, J. Chem. Phys. **55**, 1164 (1971).
- [64] E.M. Adams, I.R. McDonald, and K. Singer, Proc. R. Soc.

- London, Ser. A **357**, 37 (1977).
- [65] N. Anento and J.A. Padró, *Mol. Phys.* **99**, 275 (2001).
- [66] E.E. Shpil'rain, K.A. Yakimovich, V.A. Fomin, S.N. Skovorodjko, and A.G. Mozgovoi, *Handbook of Thermodynamic and Transport Properties of Alkali Metals*, edited by R.W. Ohse (Blackwell, Oxford, 1985), p. 753.
- [67] M. Shimoji and I. Itami, *Atomic Transport in Liquid Metals* (Trans. Tech., Aedermannsdorf, 1986).